Comparative Study of Temperature, Radiation and Mass Transfer based Models for Estimation of Reference Evapotranspiration in Iran's Northern Regions

Mohammad Poorrajabali^{1*}, Jalal Shiri^{1,2}, Sepideh Karimi¹, Amir Hossein

¹Water Engineering Department, Faculty of Agriculture, University of Tabriz, Tabriz, Iran.

²Water Engineering and Science Research Institute (WESRI), University of Tabriz, Tabriz, Iran.

*Corresponding author.

Abstract

Evapotranspiration is the most crucial factor in hydrological and climatic research, as well as irrigation planning and management. A straightforward technique of estimating reference evapotranspiration (ET_o) is highly desirable, particularly in developing regions where the meteorological data needed for the conventional FAO Penman-Monteith (FAO-56) approach is either unavailable or insufficient. Thus, the purpose of this study is to assess and assess various ETo estimate techniques against the FAO-56 approach and to identify the optimal ETo estimation equation among straightforward experimental techniques as a viable substitute for the FAO-56 method. Data from Northern regions of Iran were used to assess the applied models. In this research, fifteen common methods of estimating ET_o including temperature, radiation, and mass transfer-based models were used in both their original and calibrated versions. Temporal and regional calibration procedures were also performed to assess the calibration effect on modeling performance improvement. ET_o calculated from equation of Hargreaves-Samani 4 (HS4) in based on temperature methods in Talesh station (SI=0.167, NS=0.927, CRM=0.002) and equation of Turc (TU) in based on radiation methods in Babolsar station (SI=0.124, NS=0.963, CRM=0.052) and equation of Meyer (ME) in based on mass transfer methods in Ramsar station (SI=0.316, NS=0.738, CRM=0.001) with the lowest error percentage of each group showed the best estimate compared to the FAO-56 method. These findings highlight the adaptability and accuracy of HS4, Turc, and Meyer, recommending them as practical alternatives to the FAO-56 method, particularly in data-scarce regions.

Keywords: Temperature, Radiation, Mass Transfer, Evapotranspiration

Introduction

Evapotranspiration (ET) describes the total amount of water that escapes from a crop to the atmosphere by combining the transpiration from plant leaves and evaporation from soil and plant surfaces. Planning irrigation, supplying plants water requirement, reservoir water balance analysis, environmental studies, ecological modeling, etc all depend on accurate ET estimate. Typically, a lysimeter is used to measure ET. However, it is costly and time-consuming. Thus, indirect approaches which range from a variety of straightforward experimental models like radiation, temperature, humidity, and evaporation pan methods to intricate coupled methods e.g.Penman-Monteith are typically employed for this task. Allen et al. (1998) argued that the Penman-Monteith equation adopted by FAO can serve as a reference standard formula for reference ET (ET_o) estimation under wide climatic varities, worldwide. This model closely aligns with spatial and temporal climatic patterns in regions with varying elevations and climates, emphasizing its adaptability (Sadeghzadeh et al., 2024). ET_o represents the ET amount from a hypothetical grass cover (0.12m height and albedo of 0.23) that is well covered the surface without any

water limitation. Among the empirical models applied for ET₀ calcultaions, temperature, radiation-, and mass transfer-based equations have been applied worldwide under different climatic contexts. The performance accuracy of such models is highly dependent on the study region and the governing climatic conditions (Shiri, 2019). So, different models would provide different outcomes when they relied on data from diverse climatic conditions, which made it difficult to give a unique conclusion for adaptability of the equations for different regions. This has made impetus for conducting substantuiual researches on evaluating the suitability of different models for different locations. Among others, Tabari et al. (2010) conducted a comparative analysis of various ET_o equations in a humid location of Iran and stated that radiation-based models can provide better results for monthly ET₀ eatimations. Kisi (2013) compared various methods using data from stations in Turkey and stated that Copais and Valiantzas methods provided better estuimations of ET₀. Chatzithomas and Alexandris (2015) developed an empirical formula using solar radiation and relative humidity for ET₀ estimation and compared with other models. They found that the developed model can simulate ET₀ values in both seasonal and yearly basis, well. Bourletsikas et al. (2017) compared 24 ET₀ estimation equations for a mediteranian forest and concluded that Copais and Hargreaves models outperformed the rest of the applied equations. Antonopoulos and Antonopoulos (2017) compared various models for estimation of ET₀ in Greece and stated that Makkink and Priestley-Taylor models showed closer estimates to the FAO-PM model. Farzanpour et al. (2019) evaluated 20 ET₀ equations in a semi-arid region of Iran and found that the potential for usage of a specified model depends highly on data availability as well as the climatic conditions of the study region. Valle Junior et al. (2020) evaluated 21 equations in a tropical semi-humid region of Brazilia and reported that radiation-based models presented the most accurate results, followed by the temperature-based and masss transfer-based results (the later gave the highest error). Sharafi and Mohammadi Ghaleni (2021) used 23 empirical equations for ET₀ estimations under different climatic conditions of Iran and compared the original models with the calibrated versions. The results showed that the calibration procedure imporved the performance accuracy of the applied models to great extent. This study utilizes meteorological data from the humid climate of northern Iran to conduct a comprehensive comparison of 15 ET_o equations, categorized into three groups: temperature-based, radiation-based, and mass transfer-based methods. The primary objective is to evaluate the accuracy, adaptability, and applicability of these equations under both calibrated and non-calibrated conditions across temporal and spatial scales. A key innovation of this research lies in its dual calibration approach, combining local (station-specific) and cross-station calibrations to improve model performance and generalizability. By identifying the most reliable ET₀ estimation methods for humid climates, this study provides a practical framework for the practicioners.

MATERIALS AND METHODS

Data used

Daily climatic data from ten meteorological stations in northern Iran, recorded over an 11-years period (2010–2021), were utilized in this study. These stations are located along the coastal region of the Caspian Sea, the world's largest enclosed inland water body, and cover a diverse range of altitudes, from -23.6 meters at Bandar Anzali to 1081 meters at Masuleh (Figure 1). This variation in altitude and geographic location provides an ideal basis for analyzing the spatial and temporal variations in ET₀ under varying climatic conditions.

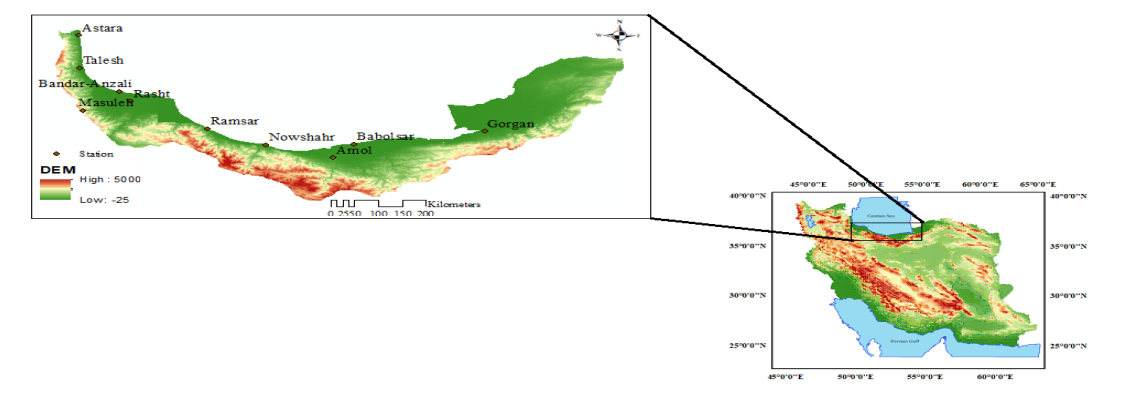


Figure 1- Study area location and distribution of stations.

The climatic parameters considered in this study (Figure 2) include mean daily temperature (T_{mean}), relative humidity (R_H), solar radiation (R_S), wind speed at 2 meters above ground (U_2), and reference evapotranspiration (ET_o). The average T_{mean} ranged from 12.19°C at Masuleh, the coldest station, to 18.27°C at Gorgan, the warmest station, with relatively stable patterns across the stations as indicated by coefficients of variation (CV) between 0.41 and 0.61. Relative humidity values ranged from 76.09% at Gorgan to 82.74% at Bandar Anzali and Rasht, with minimal variability as shown by CVs ranging from 0.09 to 0.24. Solar radiation exhibited a wider range, with daily averages between 13.12 $MJ.m^{-2}.day^{-1}$ at Bandar Anzali and 15.31 $MJ.m^{-2}.day^{-1}$ at Gorgan, and CVs between 0.47 and 0.56, highlighting moderate variability across the region. Wind speed values demonstrated notable spatial variation, ranging from 0.96 $m.s^{-1}$ at Masuleh to 2.19 $m.s^{-1}$ at Bandar Anzali, with the highest variability observed at Masuleh, where the CV reached 0.87. Finally, ET_o values ranged from 2.05 $mm.day^{-1}$ at Masuleh to 2.93 $mm.day^{-1}$ at Gorgan, with CVs between 0.61 and 0.71, reflecting the sensitivity of ET_o to changes in these climatic parameters.

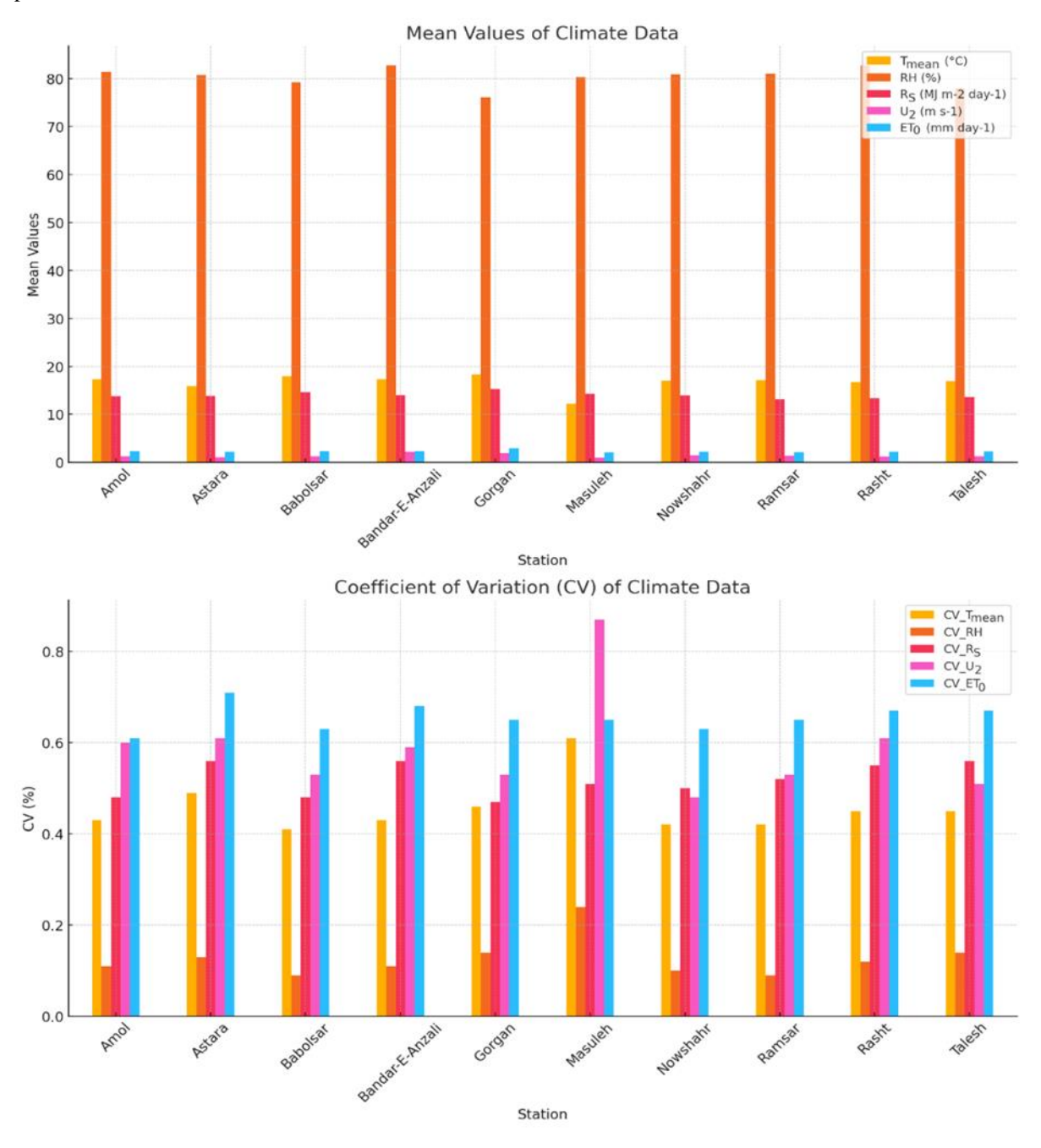


Figure 2- Mean values and coefficient of variation (CV) of climate variables across different stations.

Volume 18, No. 4, 2024

ISSN: 1750-9548

METHODS

The benchmark FAO56-PM model (Allen et al., 1998) is a commonly used appporach for calculating the ET_o values as well as calibrating the other equations:

$$ET_0 = \frac{0.408 \times \Delta (R_n - G) + \gamma \frac{900}{T_{mean} + 273} U_2(e_s - e_a)}{\Delta + \gamma (1 + 0.34 U_2)}$$
(1)

where ET₀ is the reference evapotranspiration (mm day⁻¹), Δ is the slope of the saturation vapor pressure function (kPa $^{\circ}$ C⁻¹), γ is the psychometric constant (kPa $^{\circ}$ C⁻¹), Rn is the net radiation (MJ m⁻² day⁻¹), G is the soil heat flux density (MJ m⁻² day⁻¹), T_{mean} is the mean air temperature ($^{\circ}$ C), U₂ is the average 24 h wind speed at 2 m height (m s⁻¹), e_s is the saturation vapor pressure (kPa), e_a is the actual vapor pressure (kPa), and λ is the latent heat of evaporation (MJ kg⁻¹).

In the present study, total 15 equations covering three main categories e.g. temperature-based, radiation-based and mass transfer-based were used to estimate ET_o values in the studied locations. Tables 1-3 sum up the expressions of the employed equations.

Table 1- Mathematical expressions of applied temperature-based ET_o equations.

ET _o models		Meteorological inputs	Expression
Hargreaves-Samani (2002)	HS1	Tmean, Tmax, Tmin, [Ra]	$ET_0 = 0.003 \times 0.408 R_a (T_{mean} + 20) \times (T_{max} - T_{min})^{0.4}$
HS2 (2002)		Tmean, Tmax, Tmin, [Ra]	$ET_0 = 0.0025 \times 0.408 R_a (T_{mean} + 16.8) \times (T_{max} - T_{min})^{0.5}$
HS3 (2002)		T_{mean} , T_{max} , T_{min} , P , $[R_a]$	$ET_0 = 0.0013 \times 0.408 R_a (T_{mean} + 17) \times (T_{max} - T_{min} - 0.0123 P)^{0.76}$
HS4 (2007)		T _{mean} , T _{max} , T _{min} , [R _a]	$ET_0 = 0.0023 \times 0.408 R_a (T_{mean} + 17.8) \times (T_{max} - T_{min})^{0.424}$
Schendel (1967)		T_{mean} , R_H	$ET_0 = 16 \frac{T_{mean}}{R_H}$

In these equations: ET_o =reference evapotranspiration (mm.day⁻¹), T_{mean} = mean air temperature (°C), U_2 = average 24 h wind speed at 2 m height (m.s⁻¹), R_H = relative humidity (%), P is monthly rainfall (mm), R_a = extraterrestrial radiation (mm.day⁻¹), T_{max} = maximum air temperature (°C) and T_{min} = minimum air temperature (°C).

The temperature-based equations rely primarily on air temperature and extraterrestrial radiation (R_a) to estimate ET_o . This category includes five equations: Hargreaves-Samani (HS1, HS2, HS3, and HS4) and Schendel models. These equations use meteorological inputs such as mean air temperature (T_{mean}), maximum and minimum temperatures (T_{max} , T_{min}), monthly precipitation (P), extraterrestrial radiation (R_a), and relative humidity (RH). Their simplicity makes them practical for regions with limited meteorological data availability.

Table 2- Mathematical expressions of applied radiation-based ET_o equations.

ET _o models	Meteorological inputs	Expression
Irmak et al. (2003)	T_{mean} , R_s	$ET_0 = -0.611 + 0.149 \times R_s + 0.079 \times T_{mean}$
Jones & Ritchie (1990)	Tmax, Tmin, Rs	$ET_0 = \alpha_1 [3.87 \times 10^{-3} \times R_s (0.6T_{max} + 0.4T_{min} + 29)]$
		$5 < T_{max} < 35 \qquad \alpha_I = 1.1$
		$T_{max} > 35$ $\alpha_I = 1.1 + 0.05(T_{max} - 35)$
		$T_{max} < 5$ $\alpha_1 = 0.1 \times exp[0.18(T_{max} + 20)]$
Priestley-Taylor (1972)	T_{max} , T_{min} , T_{mean} , R_S	$ET_0 = 1.26(\frac{\Delta}{\Delta + \lambda}) \frac{R_s}{\lambda}$
Makkink	T_{max} , T_{min} , T_{mean} , R_S	$ET_0 = 0.61(\frac{\Delta}{\Delta + \lambda})\frac{R_s}{\lambda} - 0.12$
Turc	Tmean, Tmax, Tmin, Rs, RH	$ET_0 = a_T \ 0.013 \left(\frac{T_{mean}}{T_{mean} + 15} \right) \left(\frac{23.8856R_s + 50}{\lambda} \right)$

$$R_{H} \geq 50 \qquad \qquad \alpha_{T} = 1$$

$$R_{H} < 50 \qquad \qquad \alpha_{T} = I + \frac{50 - R_{H}}{70}$$

In these equations: R_S = daily solar radiation (MJ.m⁻².day⁻¹), λ = latent heat of the evaporation (MJ.kg⁻¹), Δ = The slope of the saturated vapor pressure curve.

Radiation-based equations incorporate solar radiation (R_S) as a key input parameter. The five equations analyzed in this category include models proposed by Irmak et al., Jones & Ritchie, Priestley-Taylor, Makkink, and Turc. These methods utilize additional variables such as the slope of the saturation vapor pressure curve (Δ) and latent heat of evaporation (λ). Radiation-based methods are particularly effective in regions where solar radiation significantly influences evapotranspiration.

Table 3- Mathematical expressions of applied mass transfer-based ET₀ equations.

ET _o models	Meteorological inputs	Expression
Dalton (1802)	e_a , e_s , U_2	$ET_0 = (0.3648 + 0.07223U_2)(e_s - e_a)$
Trabert (1896)	e_a , e_s , U_2	$ET_0 = 0.3075 \times \sqrt{U_2} \times (e_s - e_a)$
Meyer (1926)	e_a , e_s , U_2	$ET_0 = (0.375 + 0.05026U_2)(e_s - e_a)$
Rohwer (1931)	e_a , e_S , U_2	$ET_0 = 0.44(1 + 0.27U_2).(e_s - e_a)$
WMO (1966)	e_a , e_S , U_2	$ET_0 = (0.1298 + 0.0934U_2)(e_s - e_a)$

In these equations: e_s = saturation vapor pressure, e_a = actual vapor pressure (hPa in all the equations except Rohwer models, where units are in mmHg), U_2 = average 24 h wind speed at 2 m height (m.s⁻¹).

Mass transfer-based methods emphasize the role of wind speed and vapor pressure differences in driving evapotranspiration. The equations in this category include models developed by Dalton, Trabert, Meyer, Rohwer, and WMO. They require meteorological inputs such as saturation vapor pressure (e_s) , actual vapor pressure (e_a) , and 24-hour wind speed (U_2) at 2 m height. These methods are advantageous in areas where wind and humidity data are accurately recorded.

Each of these equations was applied to ten meteorological stations across northern Iran, representing a diverse range of climatic conditions. Their performance was assessed in comparison to the benchmark FAO56-PM model. The evaluation process included both calibration and validation steps to identify the most suitable equations for the study region.

Study flowchart

The applied equations were used in their general (original) form to calculate the ET₀ in all locations. Based on previous studies, these equations might need local calibrations to adjust their coefficients before they can be successfully applied for a specified region (Shiri, 2017). However, a preliminary hypothesis might be their applicability without local calibration. So, the first step would be employing these equations at each location in their original form. Then, two calibration procedures were define to assess the models' capabilities, namely, the local and cross-station calibration. To better illustrate these calibration procedures, Figure 3 provides a schematic representation of both the locative (left) and temporal (right) calibration frameworks. The green boxes indicate the training data, while the yellow boxes represent the testing data. For the local calibration, 70% of available patterns were used for calibrating the equations, while the rest of patterns were reserved for testing. For the cross-station calibration, complete available patterns from one station were used for testing, while the remaining data

(complete patterns of 9 stations) were used for calibrating the models. The procedure was carried out for all stations.

The following equation was used to calibrate the equations in both temperal and cross-station calibration procedures:

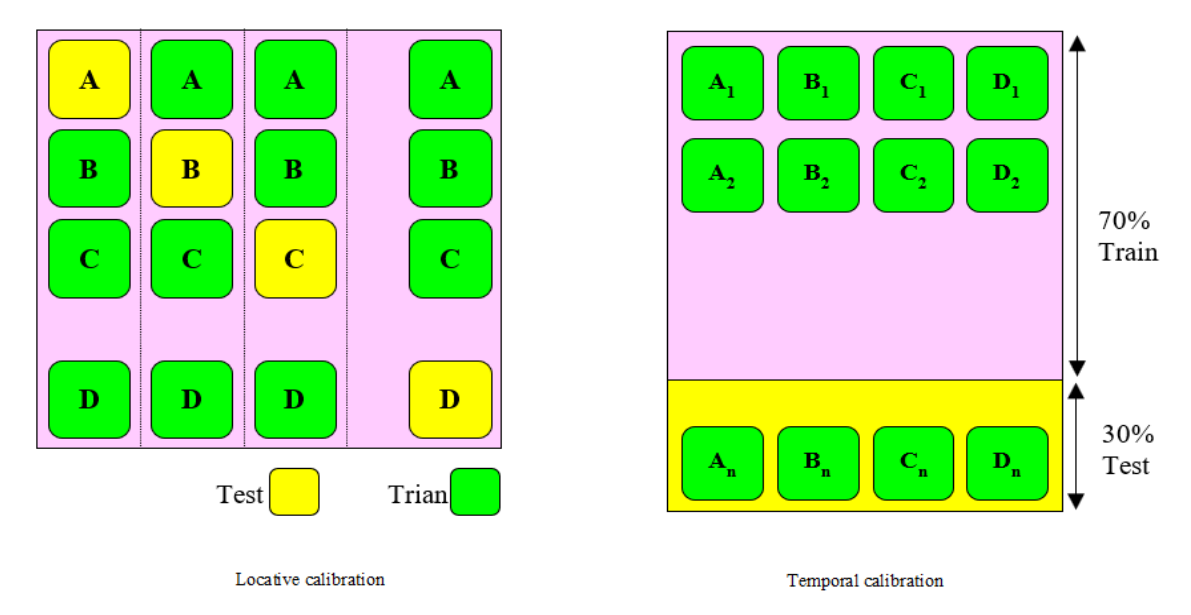


Figure 3- Illustration of locative and temporal calibration for data partitioning.

$$ET^{PM} = \alpha ET^M + b \tag{2}$$

The performance accuracy of the applied models was assessed using visual graphs as well as the statistical indices, namely, the scatter index (SI), Nash-Sutcliffe coefficient (NS) and residual mass coefficient (CRM) as follows:

$$SI = \frac{RMSE}{\overline{ET}_o} = \frac{\sqrt{\frac{1}{N}\sum_{i=1}^{N}(ET_i^M - ET_i^{PM})^2}}{\overline{ET}^{PM}}$$
(3)

$$NS = 1 - \frac{\sum_{i=1}^{N} (ET_i^{PM} - ET_i^{M})^2}{\sum_{i=1}^{N} (ET_i^{PM} - \overline{ET}^{\overline{PM}})^2}$$
(4)

$$CRM = \frac{\sum_{i=1}^{N} ET_i^{PM} - \sum_{i=1}^{N} ET_i^{M}}{\sum_{i=1}^{N} ET_i^{PM}}$$
 (5)

In the recent relations, ET_i^{PM} and ET_i^{M} are, respectively, reference evapotranspiration values in the i-th time step related to the FAO56-PM model and other used models, $\overline{ET^{PM}}$ average target ET_o values, and N is the number of patterns.

Results and Discussion

Overview of monthly ET_o variations across stations

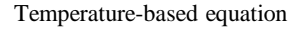
The monthly ET_o values generated by the applied models for Talesh, Babolsar, and Ramsar stations (Figures 4–6) reveal distinct seasonal trends. During the colder months (e.g., December–February), the models demonstrated close agreement, with minimal variation in estimated ET_o values. Conversely, during the warmer months (June–August), significant discrepancies emerged, with higher ET_o magnitudes and greater divergence among models. This pattern aligns with the findings from Table 4, where higher SI values during summer highlight the challenges models face in accurately estimating ET_o under extreme climatic conditions. For example, in Babolsar, the SI value for Hargreaves-Samani 4 (HS4) increased to 0.52, indicating reduced reliability under high-temperature conditions.

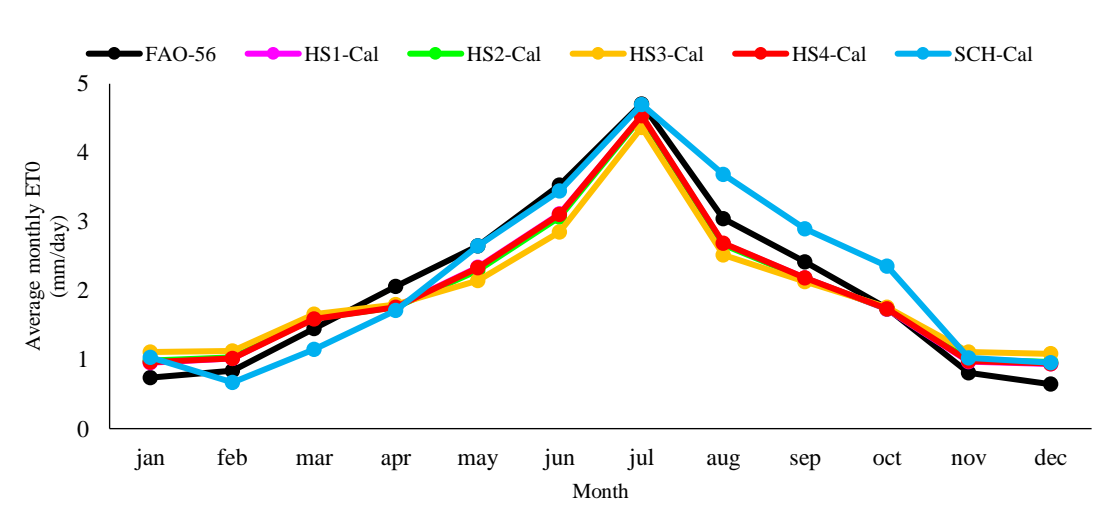
In Talesh, temperature-based models such as HS4 outperformed others, particularly during peak ET₀ months. Meanwhile, radiation-based models like Turc dominated in Babolsar, a region with high solar radiation exposure. In Ramsar, mass transfer-based models such as Meyer provided the most accurate results, reflecting the station's coastal and humid climatic characteristics.

Table 4- SI values of the ET_o models during the study period.

	Temperature-based					Radiation-based						Mass-transfer-based				
	HS1	HS2	HS3	HS4	SCH	PT	JR	MK	TU	IR	DA	TR	ME	RO	WMO	
Amol	0.224	0.238	0.310	0.224	0.326	0.266	0.169	0.266	0.147	0.153	0.328	0.370	0.326	0.333	0.374	
Astara	0.182	0.192	0.251	0.182	0.333	0.241	0.148	0.241	0.129	0.149	0.346	0.400	0.337	0.358	0.414	
Babolsar	0.210	0.234	0.346	0.213	0.321	0.246	0.148	0.246	0.124	0.149	0.387	0.407	0.383	0.392	0.424	
B-Anzali	0.201	0.226	0.344	0.205	0.355	0.250	0.155	0.250	0.146	0.156	0.364	0.384	0.361	0.370	0.408	
Gorgan	0.284	0.314	0.469	0.287	0.456	0.422	0.292	0.422	0.253	0.305	0.505	0.548	0.484	0.524	0.572	
Masuleh	0.196	0.209	0.270	0.197	0.569	0.288	0.153	0.288	0.151	0.171	0.484	0.564	0.468	0.499	0.554	
Nowshahr	0.192	0.207	0.297	0.192	0.321	0.253	0.149	0.253	0.139	0.145	0.339	0.363	0.335	0.344	0.377	
Ramsar	0.192	0.208	0.298	0.193	0.345	0.243	0.144	0.243	0.133	0.142	0.320	0.347	0.316	0.326	0.361	
Rasht	0.203	0.215	0.282	0.203	0.386	0.238	0.159	0.238	0.145	0.150	0.372	0.424	0.360	0.385	0.442	
Talesh	0.166	0.173	0.230	0.165	0.350	0.235	0.152	0.235	0.140	0.146	0.331	0.365	0.318	0.345	0.405	

Notes: HS1: Hargreaves-Samani 1; HS2: Hargreaves-Samani 2; HS3: Hargreaves-Samani 3; HS 4: Hargreaves-Samani 4; SCH: Schendel; PT: Priestley-Taylor; JR: Jones- Ritchie; MK: Makkink; TU: Turc; IR: Irmak; DA: Dalton; TR: Trabert; ME: Meyer; RO: Rohwer.





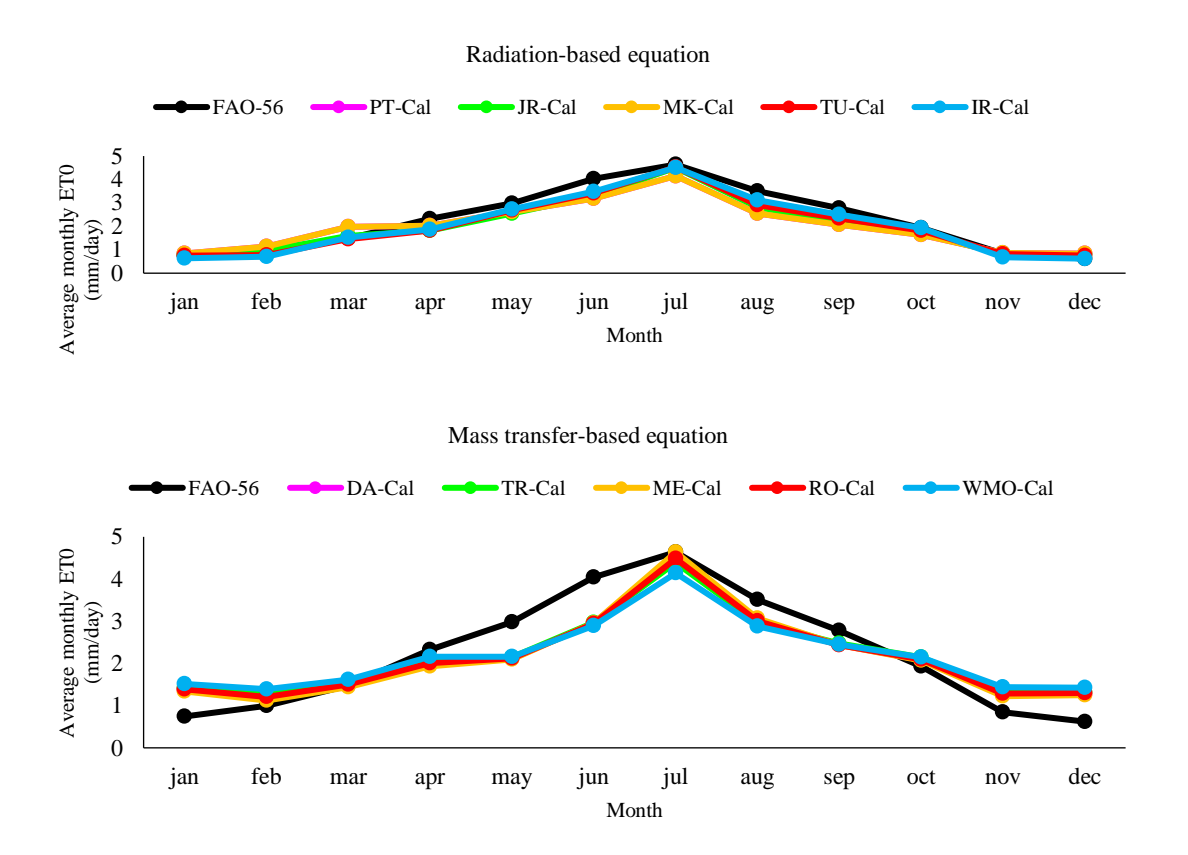
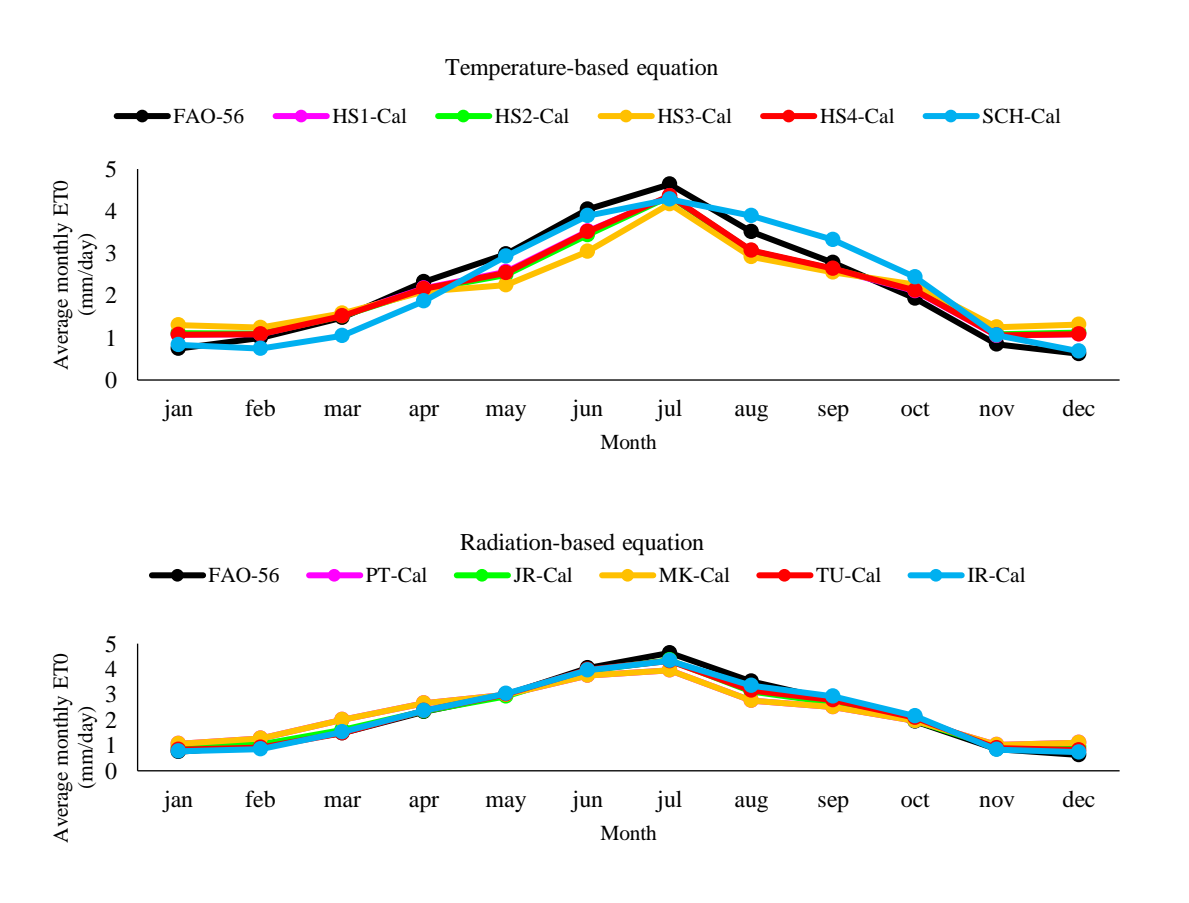


Figure 4- Average monthly ET_{o} values of different models for Talesh station.



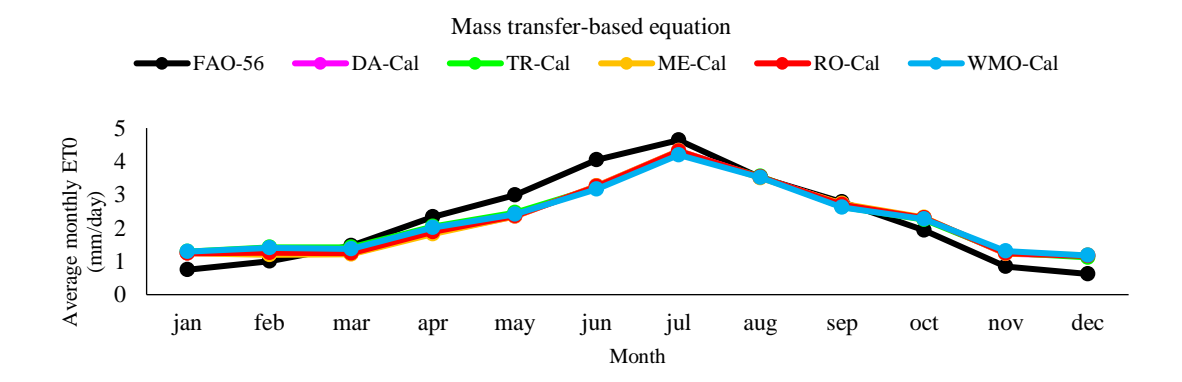
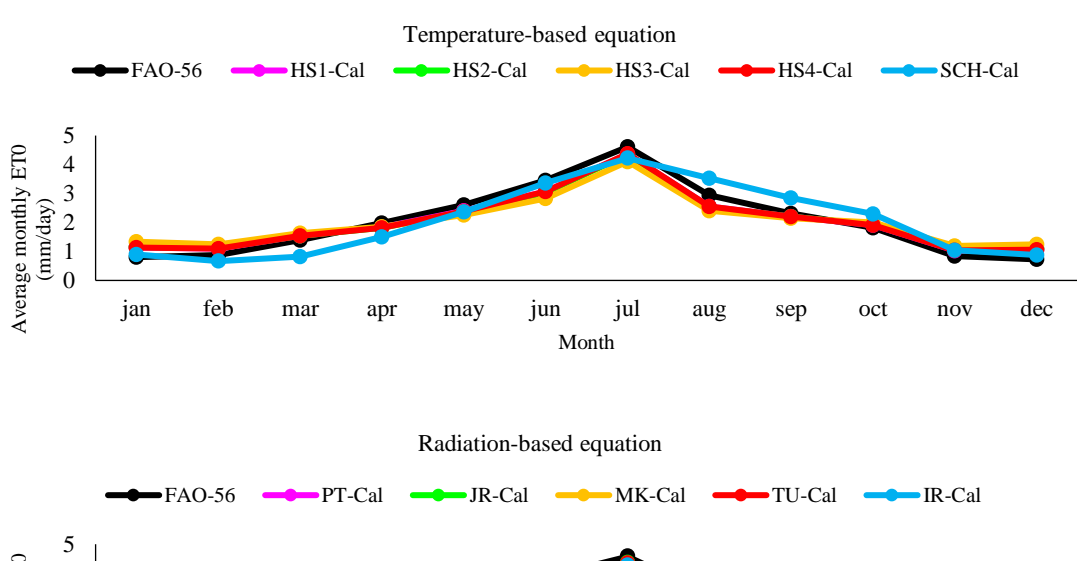
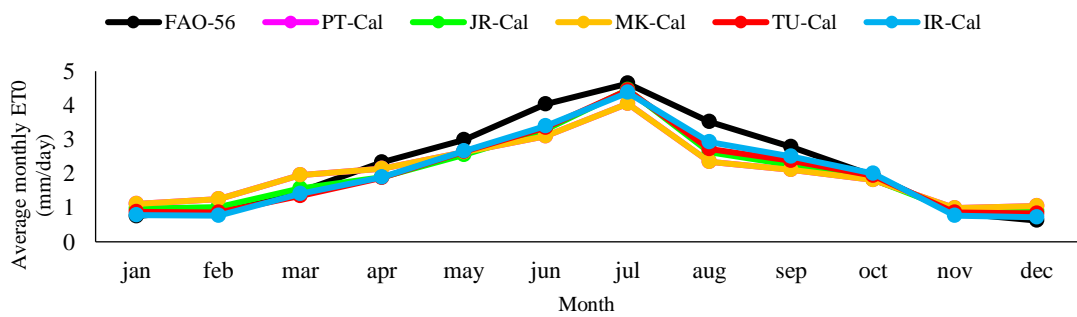


Figure 5- Average monthly ET_o values of different equations in Babolsar station.





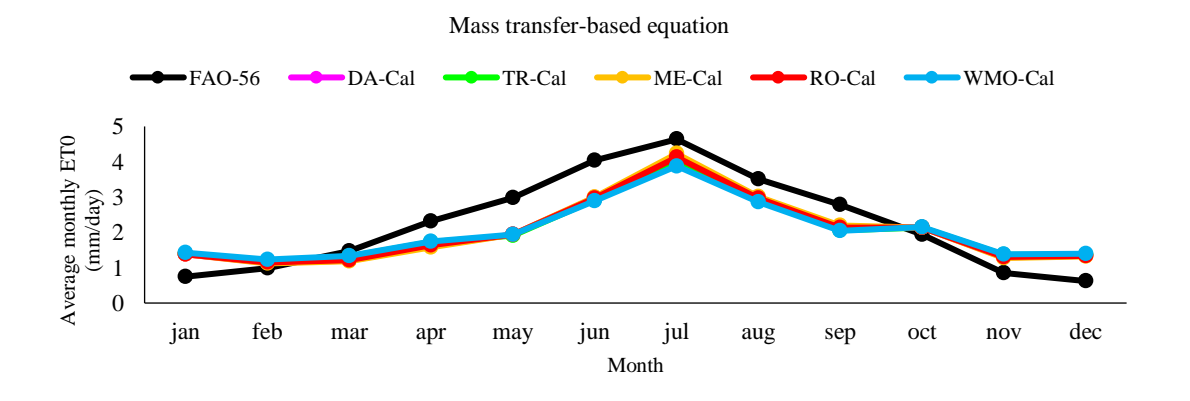


Figure 6- Average monthly ET₀ values of different equations in Ramsar station.

Performance of temperature-based models

Temperature-based models, including the Hargreaves-Samani (HS1–HS4) series and Schendel (SCH), exhibited varying levels of accuracy across stations. Table 5 highlights that the highest SI value among temperature-based models was achieved by HS4 in Talesh, with a value of 0.165 during temporal calibration, confirming its superior adaptability to regional conditions. HS4 consistently outperformed its counterparts, with SI, NS, and CRM values of 0.165, 0.939, and 0.002, respectively, in Talesh under locative calibration (Figures 7–12). This demonstrates its robustness in capturing the influence of temperature on ET_o. Similarly, HS1 showed strong performance in Babolsar, achieving SI, NS, and CRM values of 0.204, 0.901, and -0.016 under temporal calibration.

The SCH model underperformed significantly, with high SI values across stations (e.g., 0.569 in Masuleh), indicating excessive scatter in its predictions. This discrepancy is likely due to the model's incorporation of wind speed, which introduces additional variability without adequately accounting for localized conditions.

Calibration played a critical role in enhancing the performance of temperature-based models. HS4, for instance, saw a 30% improvement in SI values post-calibration (Table 6), particularly in locative scenarios, underscoring its adaptability to diverse climatic conditions.

Table 5- SI values of the ET_o models during the temporal calibration.

		Temp	erature-	-based			Rad	iation-b	ased		Mass-transfer-based				
	HS1	HS2	HS3	HS4	SCH	PT	JR	MK	TU	IR	DA	TR	ME	RO	WMO
	Calibrated														
Amol	0.221	0.234	0.305	0.221	0.317	0.263	0.166	0.263	0.145	0.152	0.316	0.394	0.314	0.321	0.365
Astara	0.177	0.186	0.240	0.177	0.345	0.247	0.154	0.247	0.140	0.158	0.309	0.354	0.307	0.315	0.356
Babolsar	0.204	0.221	0.318	0.205	0.295	0.252	0.144	0.252	0.127	0.134	0.342	0.349	0.345	0.342	0.357
B-Anzali	0.165	0.178	0.271	0.165	0.325	0.257	0.156	0.257	0.143	0.159	0.347	0.369	0.340	0.355	0.394
Gorgan	0.272	0.289	0.372	0.272	0.387	0.341	0.218	0.341	0.201	0.208	0.310	0.312	0.313	0.311	0.340
Masuleh	0.170	0.175	0.212	0.170	0.336	0.238	0.179	0.238	0.145	0.162	0.369	0.411	0.350	0.385	0.432
Nowshahr	0.185	0.196	0.268	0.185	0.315	0.249	0.141	0.249	0.117	0.127	0.316	0.329	0.316	0.317	0.336
Ramsar	0.176	0.186	0.256	0.176	0.316	0.239	0.136	0.239	0.117	0.130	0.300	0.324	0.298	0.304	0.332
Rasht	0.195	0.207	0.270	0.196	0.346	0.239	0.160	0.239	0.142	0.156	0.340	0.388	0.332	0.349	0.399
Talesh	0.168	0.174	0.221	0.167	0.317	0.236	0.154	0.236	0.134	0.142	0.300	0.323	0.287	0.314	0.371
						No	on-Cali	brated							
Amol	0.630	0.610	0.547	0.309	0.412	0.814	0.349	0.272	0.642	0.256	0.625	0.445	0.567	1.089	0.433
Astara	0.617	0.579	0.450	0.269	0.417	0.804	0.374	0.253	0.633	0.264	0.556	0.397	0.498	0.999	0.448
Babolsar	0.478	0.412	0.359	0.216	0.431	0.833	0.402	0.265	0.641	0.300	0.440	0.360	0.403	0.807	0.506
B-Anzali	0.405	0.335	0.353	0.194	0.428	0.831	0.396	0.260	0.645	0.283	0.504	0.428	0.420	0.960	0.461
Gorgan	0.790	0.814	0.830	0.375	0.395	1.103	0.299	0.439	0.900	0.230	1.328	1.006	1.111	2.288	0.545
Masuleh	0.411	0.381	0.334	0.201	0.467	0.657	0.242	0.185	0.556	0.189	0.752	0.687	0.627	1.243	0.608
Nowshahr	0.489	0.433	0.352	0.222	0.444	0.769	0.367	0.251	0.599	0.282	0.476	0.358	0.424	0.866	0.443
Ramsar	0.419	0.365	0.328	0.203	0.535	0.743	0.334	0.243	0.578	0.276	0.564	0.390	0.502	0.991	0.411
Rasht	0.646	0.624	0.542	0.304	0.406	0.799	0.358	0.247	0.629	0.254	0.551	0.428	0.501	0.953	0.508
Talesh	0.526	0.483	0.360	0.234	0.602	0.780	0.310	0.247	0.606	0.260	0.829	0.569	0.714	1.416	0.457

Notes: HS1: Hargreaves-Samani 1; HS2: Hargreaves-Samani 2; HS3: Hargreaves-Samani 3; HS 4: Hargreaves-Samani 4; SCH: Schendel; PT: Priestley-Taylor; JR: Jones- Ritchie; MK: Makkink; TU: Turc; IR: Irmak; DA: Dalton; TR: Trabert; ME: Meyer; RO: Rohwer.

Table 6 - NS values of the ET_o models during the temporal calibration.

	Temperature-based						Radia	ation-b	ased		Mass-transfer-based				
	HS1	HS2	HS3	HS4	SCH	PT	JR	MK	TU	IR	DA	TR	ME	RO	WMO
	Calibrated														
Amol	0.862	0.845	0.738	0.862	0.718	0.806	0.922	0.806	0.941	0.935	0.719	0.564	0.723	0.710	0.625
Astara	0.931	0.924	0.873	0.931	0.738	0.865	0.948	0.865	0.957	0.945	0.789	0.724	0.793	0.782	0.720

Volume 18, No. 4, 2024

ISSN: 1750-9548

Babolsar	0.901	0.883	0.759	0.900	0.792	0.849	0.950	0.849	0.962	0.957	0.721	0.710	0.717	0.721	0.695
B-Anzali	0.941	0.931	0.840	0.941	0.771	0.857	0.947	0.857	0.956	0.945	0.739	0.704	0.749	0.726	0.661
Gorgan	0.899	0.887	0.812	0.899	0.796	0.842	0.935	0.842	0.945	0.941	0.869	0.868	0.867	0.868	0.843
Masuleh	0.899	0.894	0.844	0.900	0.606	0.804	0.888	0.804	0.927	0.909	0.527	0.413	0.574	0.483	0.349
Nowshahr	0.905	0.893	0.801	0.906	0.727	0.829	0.945	0.829	0.962	0.955	0.724	0.702	0.724	0.722	0.688
Ramsar	0.909	0.898	0.807	0.909	0.706	0.832	0.946	0.832	0.960	0.950	0.735	0.691	0.739	0.728	0.675
Rasht	0.906	0.895	0.820	0.906	0.704	0.859	0.937	0.859	0.951	0.940	0.715	0.628	0.728	0.699	0.605
Talesh	0.927	0.921	0.873	0.927	0.739	0.855	0.939	0.855	0.953	0.948	0.767	0.728	0.786	0.744	0.641
Non-Calibrated															
Amol	-0.118	-0.045	0.157	0.731	0.523	-0.864	0.658	0.791	-0.160	0.815	-0.098	0.442	0.095	-2.336	0.471
Astara	0.163	0.263	0.554	0.841	0.617	-0.424	0.692	0.859	0.117	0.847	0.319	0.653	0.455	-1.197	0.557
Babolsar	0.455	0.595	0.692	0.889	0.558	-0.654	0.615	0.832	0.018	0.785	0.537	0.690	0.612	-0.553	0.389
B-Anzali	0.644	0.756	0.730	0.918	0.602	-0.499	0.660	0.854	0.098	0.826	0.449	0.603	0.617	-0.998	0.537
Gorgan	0.150	0.097	0.062	0.809	0.788	-0.656	0.878	0.737	-0.103	0.928	-1.398	-0.377	-0.680	-6.122	0.596
Masuleh	0.412	0.496	0.611	0.860	0.242	-0.502	0.797	0.881	-0.075	0.876	-0.968	-0.640	-0.365	-4.371	-0.286
Nowshahr	0.339	0.482	0.658	0.864	0.455	-0.634	0.627	0.825	0.009	0.780	0.373	0.646	0.502	-1.075	0.456
Ramsar	0.484	0.608	0.684	0.878	0.159	-0.623	0.672	0.826	0.017	0.776	0.066	0.552	0.260	-1.889	0.503
Rasht	-0.029	0.039	0.276	0.772	0.593	-0.575	0.684	0.849	0.022	0.841	0.251	0.548	0.381	-1.242	0.363
Talesh	0.281	0.393	0.663	0.857	0.058	-0.580	0.751	0.841	0.044	0.825	-0.786	0.159	-0.327	-4.212	0.457

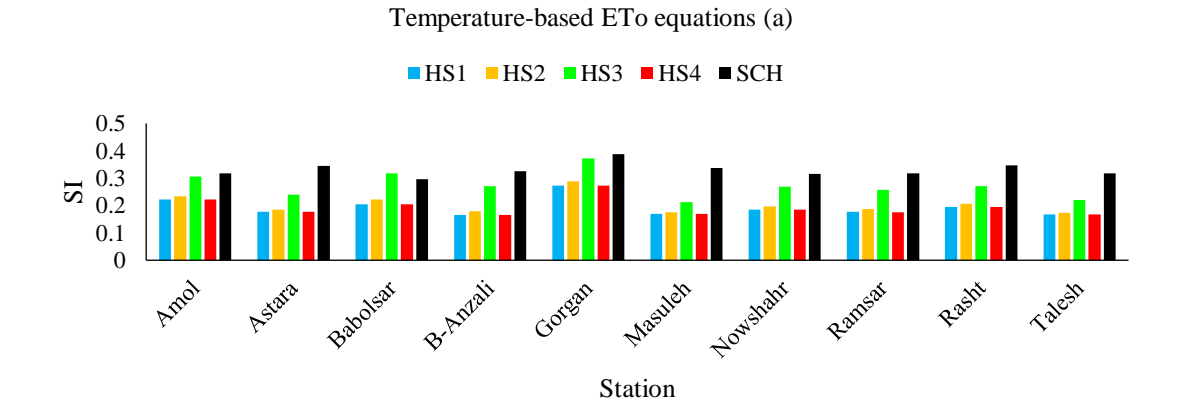
Notes: HS1: Hargreaves-Samani 1; HS2: Hargreaves-Samani 2; HS3: Hargreaves-Samani 3; HS 4: Hargreaves-Samani 4; SCH: Schendel; PT: Priestley-Taylor; JR: Jones- Ritchie; MK: Makkink; TU: Turc; IR: Irmak; DA: Dalton; TR: Trabert; ME: Meyer; RO: Rohwer.

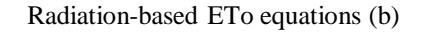
Radiation-based models: The dominance of Turc

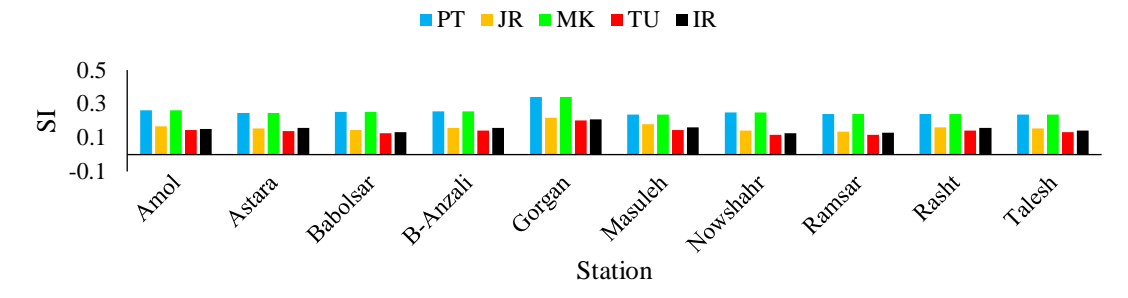
Radiation-based models demonstrated their strength in stations with high solar radiation influence. The Turc model emerged as the most reliable, achieving the lowest SI (0.117), highest NS (0.962), and minimal CRM (-0.009) in Nowshahr during temporal calibration. Figures 7–9 highlight the consistent performance of Turc across multiple stations, even outperforming the FAO-56 method in some cases. Table 4 further supports this finding, showing that Turc maintained an SI value of 0.17 across coastal stations, ensuring stable performance.

The Irmak and Jones-Ritchie models also displayed strong performance in regions like Ramsar, with SI values of 0.149 and 0.146, respectively. However, models like Priestley-Taylor (PT) and Makkink (MK) showed moderate accuracy, with higher SI values and suboptimal CRM results, suggesting their limited applicability in humid regions like northern Iran.

Calibration significantly enhanced the performance of radiation-based models, particularly for Turc. Locative calibration (Figures 10–12) revealed its transferability across stations, making it a robust alternative to the FAO-56 method in data-scarce scenarios.







Mass transfer-based ETo equations (c)

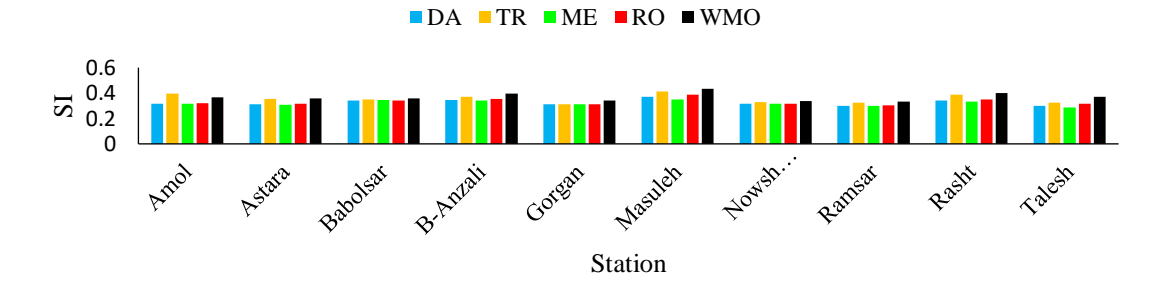
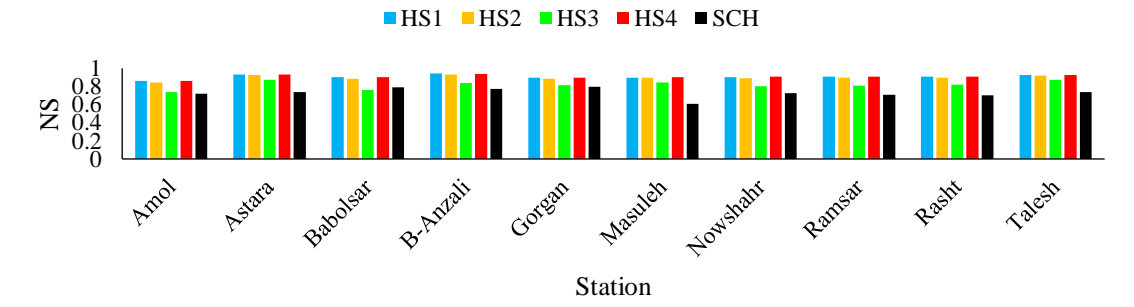
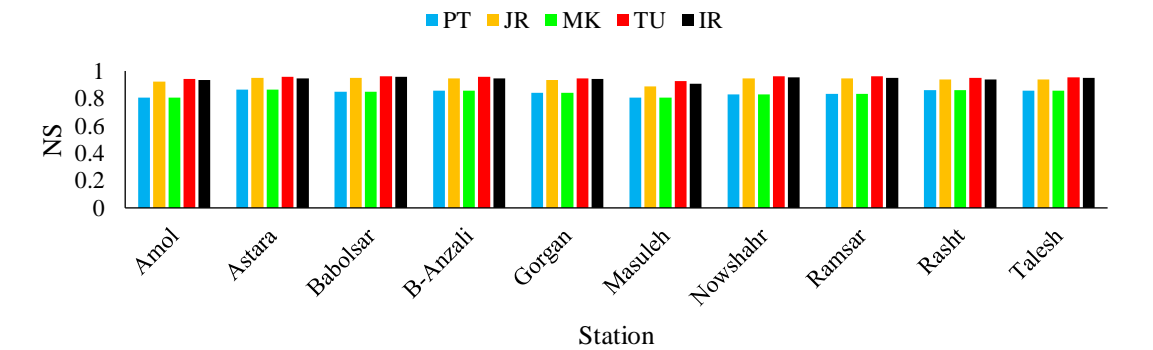


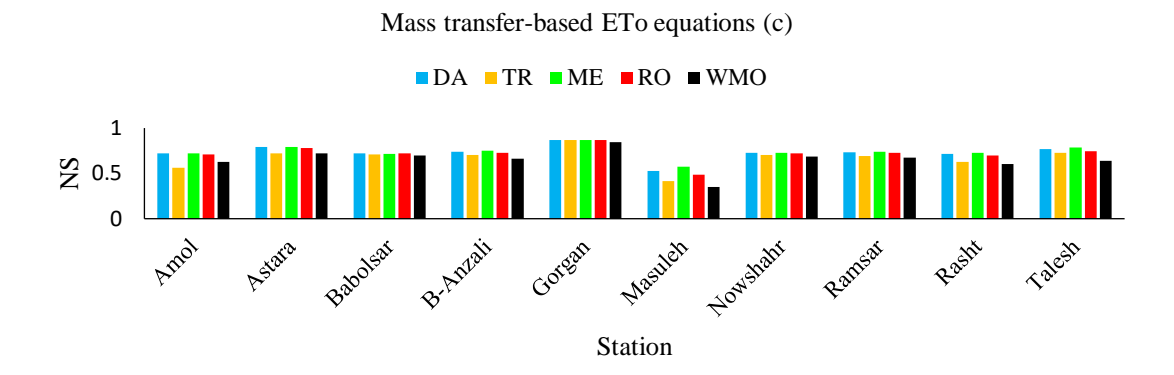
Figure 7- SI values of the temporal calibrated models.

Temperature-based ETo equations (a)



Radiation-based ETo equations (b)





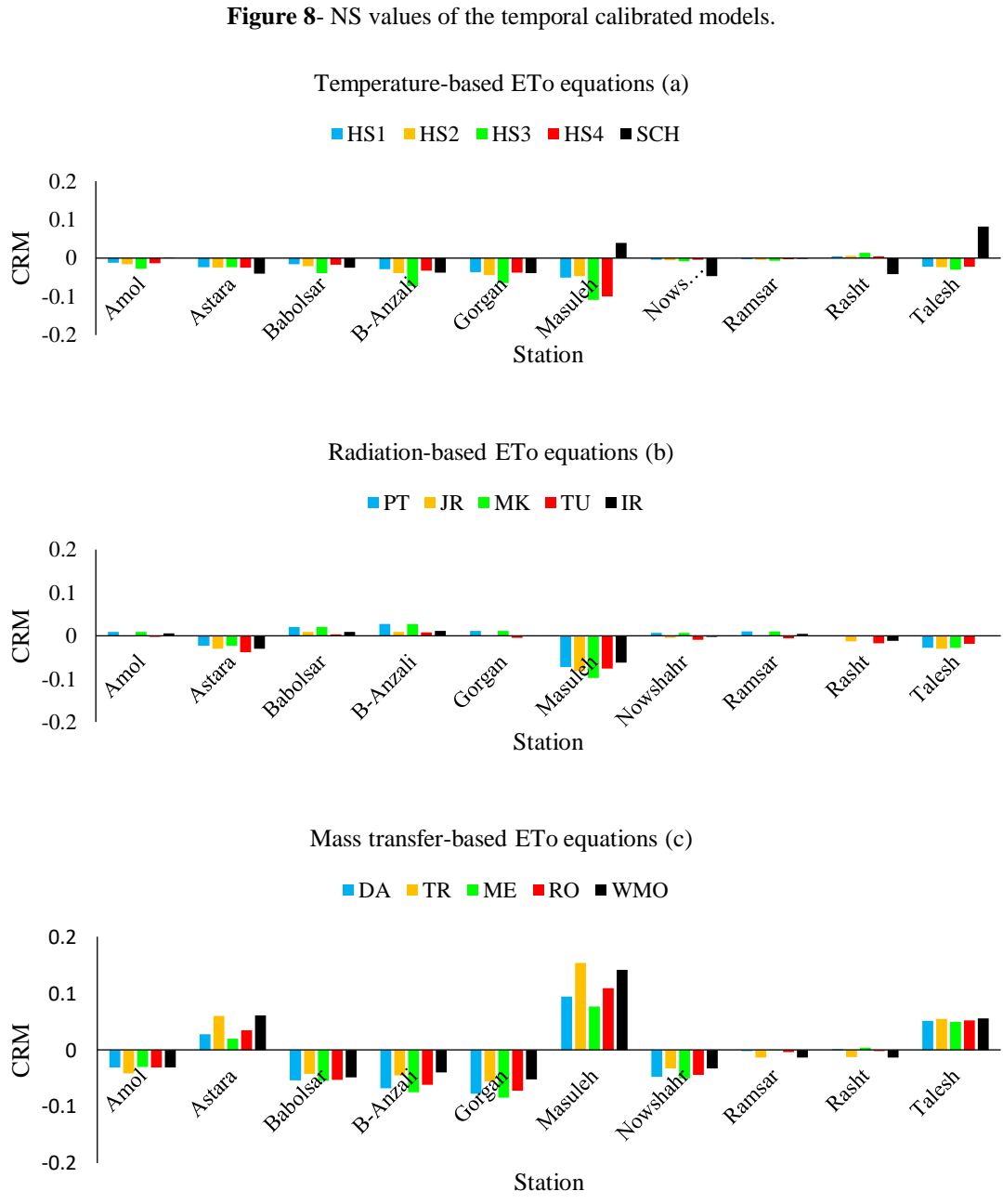
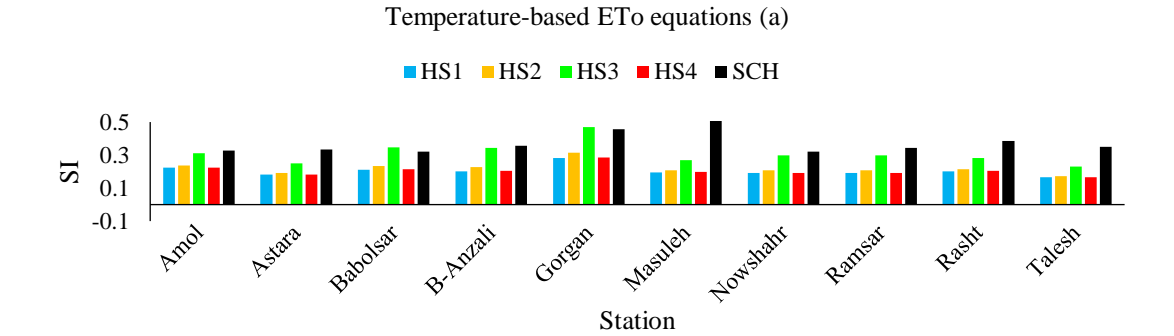
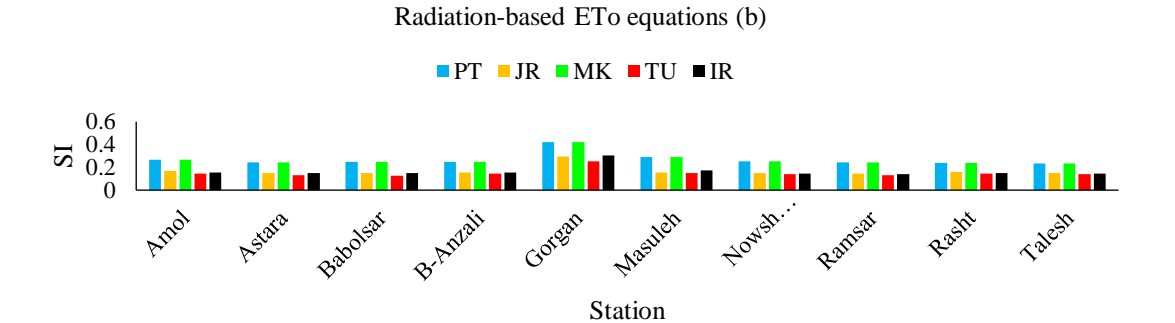


Figure 9 - CRM values of the temporal calibrated models.





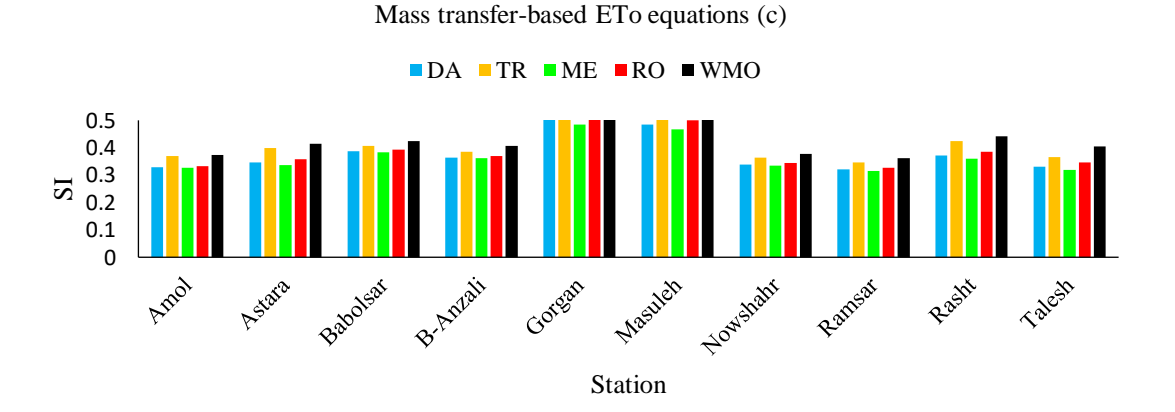
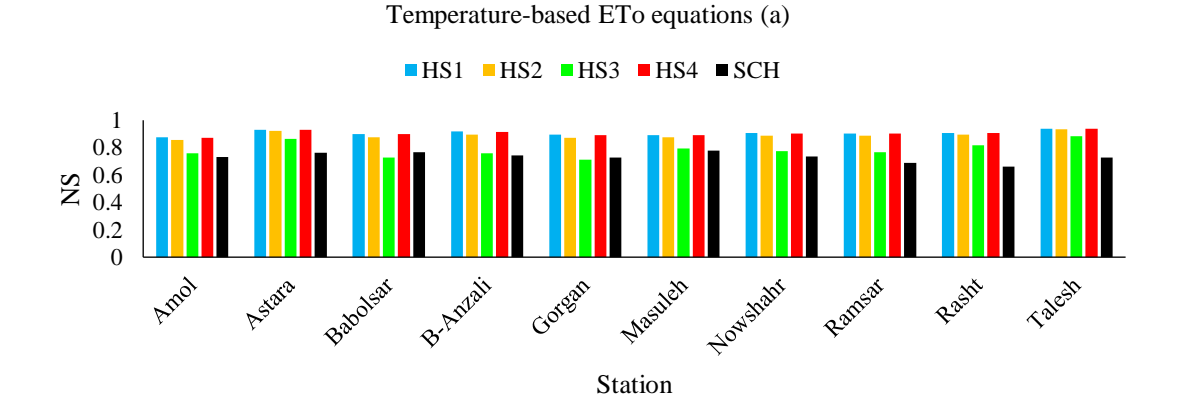
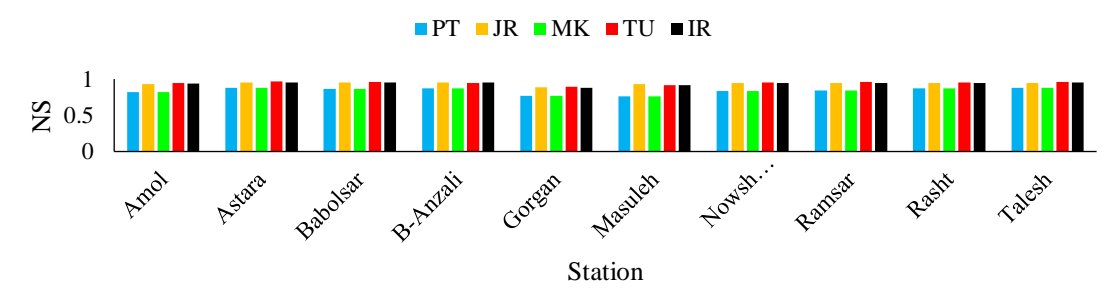


Figure 10 - SI values of the locative calibrated models.







Mass transfer-based ETo equations (c)

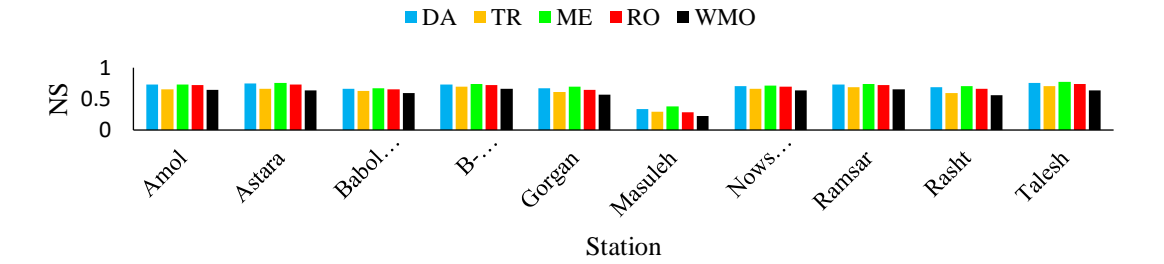
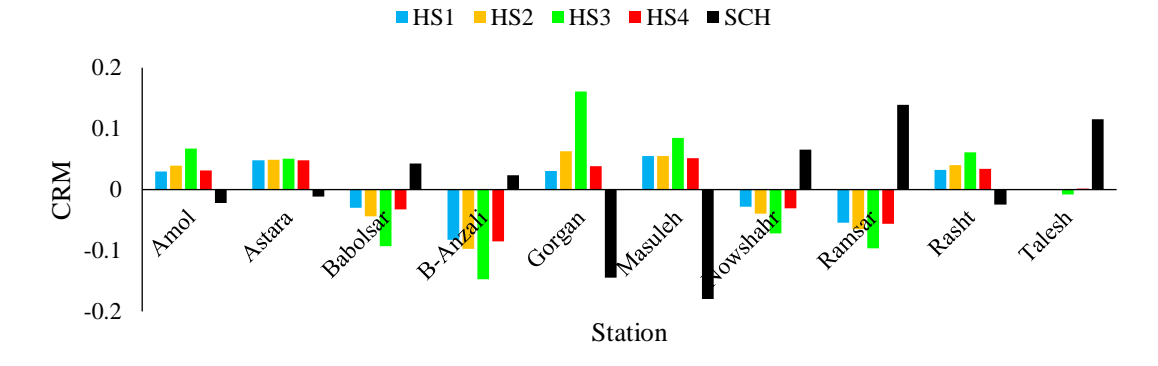
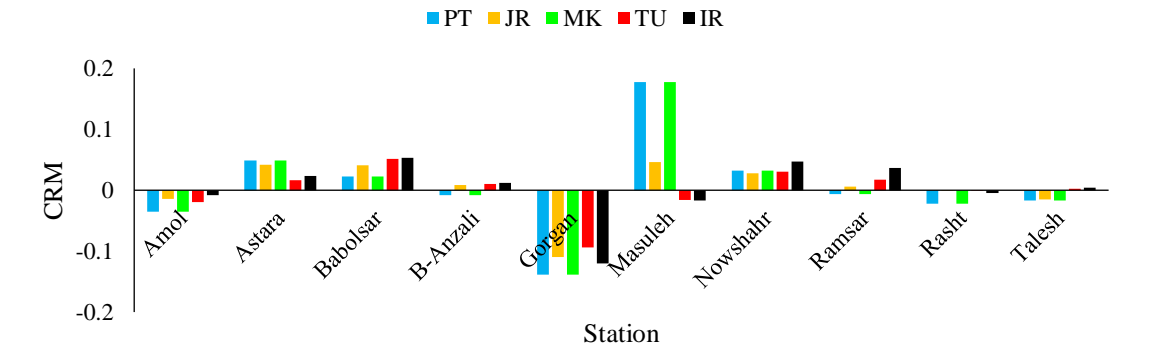


Figure 11- NS values of the licative calibrated models.

Temperature-based ETo equations (a)



Radiation-based ETo equations (b)



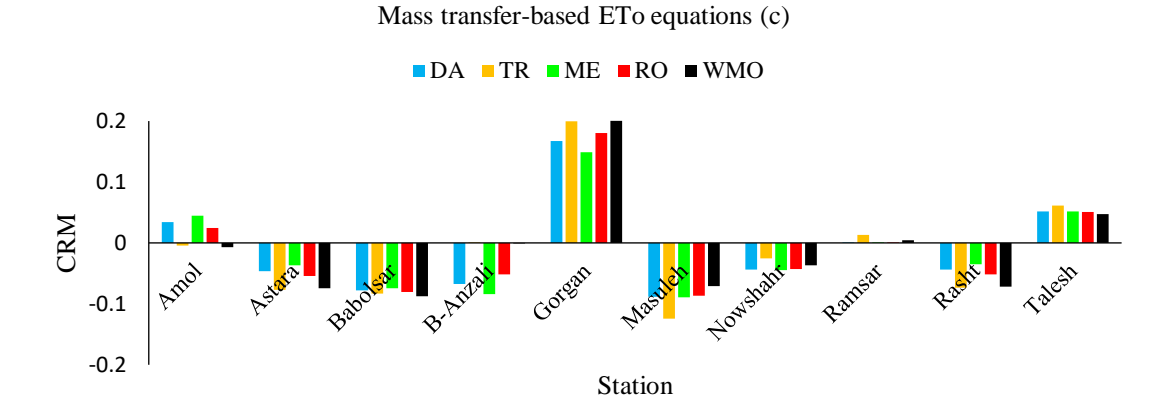


Figure 12- CRM values of the locative calibrated models.

Mass transfer-based models: The reliability of Meyer

Among mass transfer-based models, Meyer (ME) consistently delivered superior accuracy, particularly in Ramsar, with SI, NS, and CRM values of 0.298, 0.738, and 0.001, respectively, during temporal calibration. Dalton (DA) also demonstrated reasonable accuracy in select stations, such as Astara and Talesh, under locative calibration. As shown in Table 5, Meyer achieved the highest SI values among mass transfer-based models, indicating its reliability in coastal and humid conditions.

In contrast, the WMO method showed the poorest performance across all stations, with SI values exceeding 0.5 in multiple locations, highlighting its lack of precision. The high variability observed in mass transfer-based methods may be attributed to their reliance on wind speed and vapor pressure, which can exhibit substantial fluctuations in coastal regions.

Calibration markedly improved the reliability of Meyer and Dalton, reducing SI values by 25–30% across stations (Figures 7–12). Table 7 further highlights this improvement, with CRM values for Meyer decreasing to near-zero levels, indicating minimal bias post-calibration. This underscores the importance of calibration in adapting mass transfer-based methods to specific regional conditions.

	Temp	eratur	e-based	l		Radiat	ion-ba	sed			Mass-transfer-based				
	HS1	HS2	HS3	HS4	SCH	PT	JR	MK	TU	IR	DA	TR	ME	RO	WMO
Calibrated															
Amol	-0.012	-0.016	-0.027	-0.014	0.001	0.010	-0.001	0.010	-0.002	0.005	-0.031	-0.042	-0.031	-0.031	-0.031
Astara	-0.024	-0.024	-0.024	-0.024	-0.041	-0.023	-0.030	-0.023	-0.039	-0.030	0.027	0.060	0.020	0.035	0.061
Babolsar	-0.016	-0.022	-0.040	-0.018	-0.025	0.020	0.009	0.020	0.004	0.009	-0.054	-0.042	-0.055	-0.053	-0.049
B-Anzali	-0.029	-0.039	-0.073	-0.032	-0.038	0.027	0.009	0.027	0.007	0.012	-0.068	-0.045	-0.075	-0.061	-0.040
Gorgan	-0.036	-0.044	-0.065	-0.038	-0.039	0.011	-0.001	0.011	-0.004	0.000	-0.078	-0.056	-0.084	-0.072	-0.052
Masuleh	-0.121	-0.117	-0.108	-0.119	0.039	-0.173	-0.151	-0.173	-0.096	-0.122	0.094	0.153	0.077	0.109	0.141
Nowshahr	-0.004	-0.005	-0.008	-0.005	-0.047	0.007	-0.005	0.007	-0.009	-0.002	-0.047	-0.032	-0.050	-0.044	-0.033
Ramsar	-0.003	-0.004	-0.007	-0.003	-0.001	0.010	-0.001	0.010	-0.005	0.004	-0.002	-0.014	0.001	-0.004	-0.013
Rasht	0.005	0.006	0.014	0.005	-0.042	0.000	-0.013	0.000	-0.018	-0.012	0.001	-0.013	0.004	-0.002	-0.014
Talesh	-0.023	-0.024	-0.030	-0.023	0.082	-0.027	-0.030	-0.027	-0.018	-0.001	0.051	0.055	0.050	0.053	0.055

Table 7- CRM values of the ET_o models during the temporal calibration.

Non-Calibrated

Amol	0.401	0.348	0.154	0.071	0.250	-0.651	0.253	-0.051 -0.528	3 0.196	0.425	0.022 0.370	0.843	-0.227
Astara	0.402	0.337	0.108	0.070	0.228	-0.634	0.289	-0.004 -0.517	7 0.204	0.324	-0.038 0.273	0.713	-0.280
Babolsar	0.315	0.227	-0.080	-0.001	0.296	-0.634	0.322	-0.003 -0.497	7 0.251	0.218	-0.087 0.167	0.582	-0.326
B-Anzali	0.218	0.122	-0.206	-0.077	0.268	-0.639	0.289	-0.018 -0.508	3 0.219	0.205	0.025 0.117	0.614	-0.228

Volume 18, No. 4, 2024

ISSN: 1750-9548

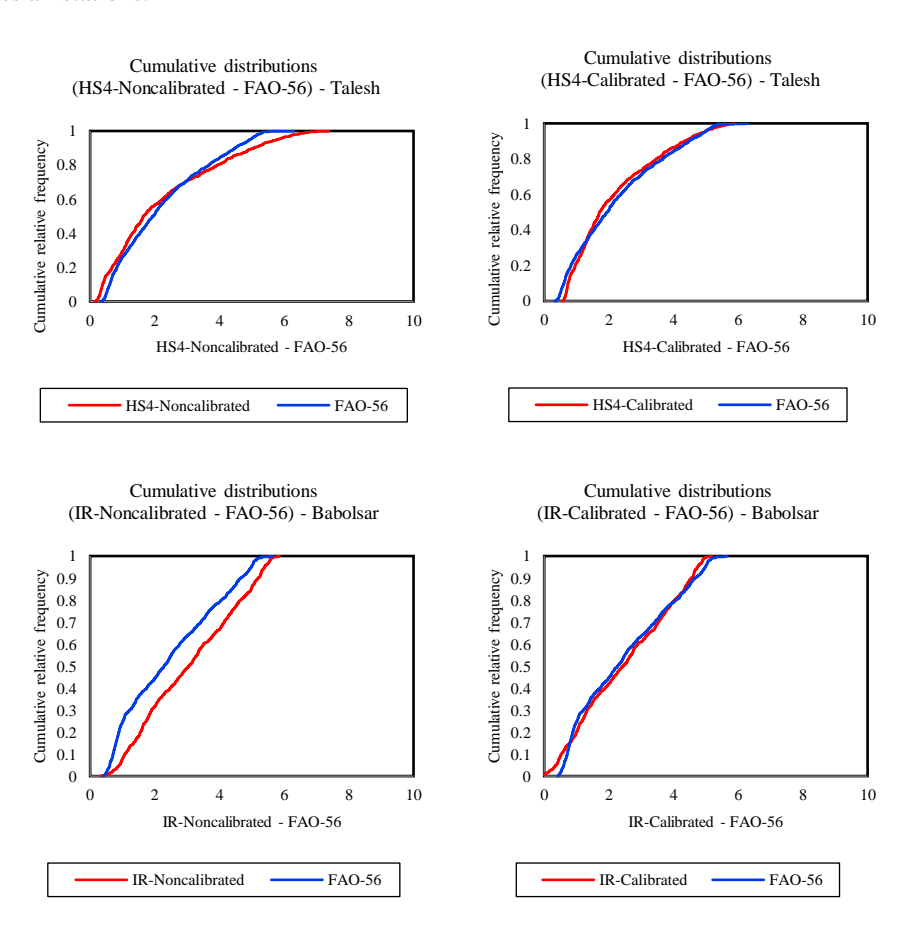
Gorgan	0.421	0.406	0.312	0.096	0.077	-0.690	0.143	-0.152	-0.575 0.058	0.751	0.491 0.621	1.349	0.129
Masuleh	0.236	0.161	-0.050	-0.065	0.151	-0.629	0.179	0.002	-0.562 0.103	0.317	0.061 0.228	0.754	-0.177
Nowshahr	0.314	0.229	-0.057	-0.002	0.308	-0.630	0.299	0.005	-0.505 0.249	0.246	-0.034 0.187	0.627	-0.291
Ramsar	0.263	0.174	-0.122	-0.042	0.431	-0.637	0.279	-0.017	-0.508 0.252	0.352	0.015 0.295	0.756	-0.252
Rasht	0.416	0.364	0.173	0.083	0.215	-0.647	0.259	-0.042	-0.525 0.192	0.306	-0.086 0.265	0.678	-0.316
Talesh	0.326	0.256	0.005	0.011	0.482	-0.651	0.225	-0.055	-0.519 0.213	0.536	0.199 0.458	1.011	-0.115

Notes: HS1: Hargreaves-Samani 1; HS2: Hargreaves-Samani 2; HS3: Hargreaves-Samani 3; HS 4: Hargreaves-Samani 4; SCH: Schendel; PT: Priestley-Taylor; JR: Jones- Ritchie; MK: Makkink; TU: Turc; IR: Irmak; DA: Dalton; TR: Trabert; ME: Meyer; RO: Rohwer.

Cumulative distribution of calibrated models

Figures 13 and 14 provide a comparative analysis of the cumulative distribution of calibrated and non-calibrated models. The HS4 model displayed minimal differences between its calibrated and non-calibrated forms, reaffirming its inherent robustness. Conversely, models based on radiation and mass transfer exhibited significant improvements post-calibration, with narrower distributions and closer alignment to the FAO-56 benchmark. This is further supported by Table 6, where the NS values for HS4 reached 0.94 post-calibration, indicating a strong fit with observed data.

These findings highlight the critical role of calibration in enhancing model performance, particularly for radiation and mass transfer-based approaches. Calibration effectively reduced biases and improved the reliability of ET_o estimates across all stations.



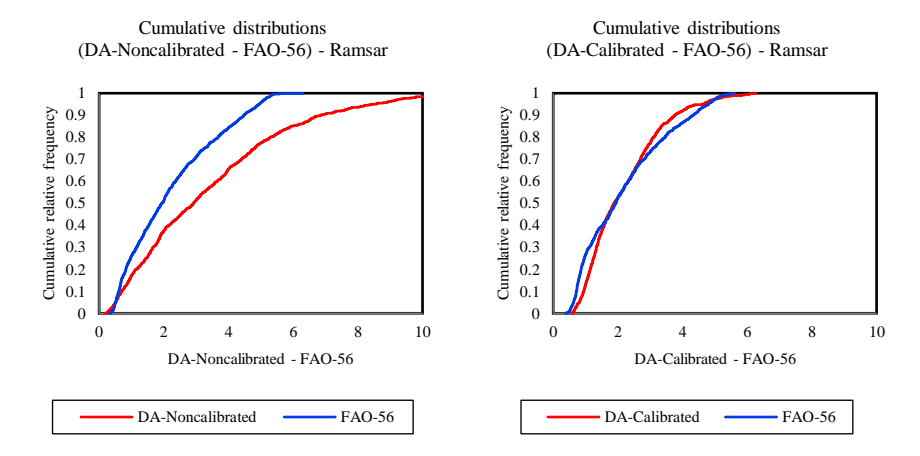


Figure 13- Cumulative distribution of the temporal calibrated models.

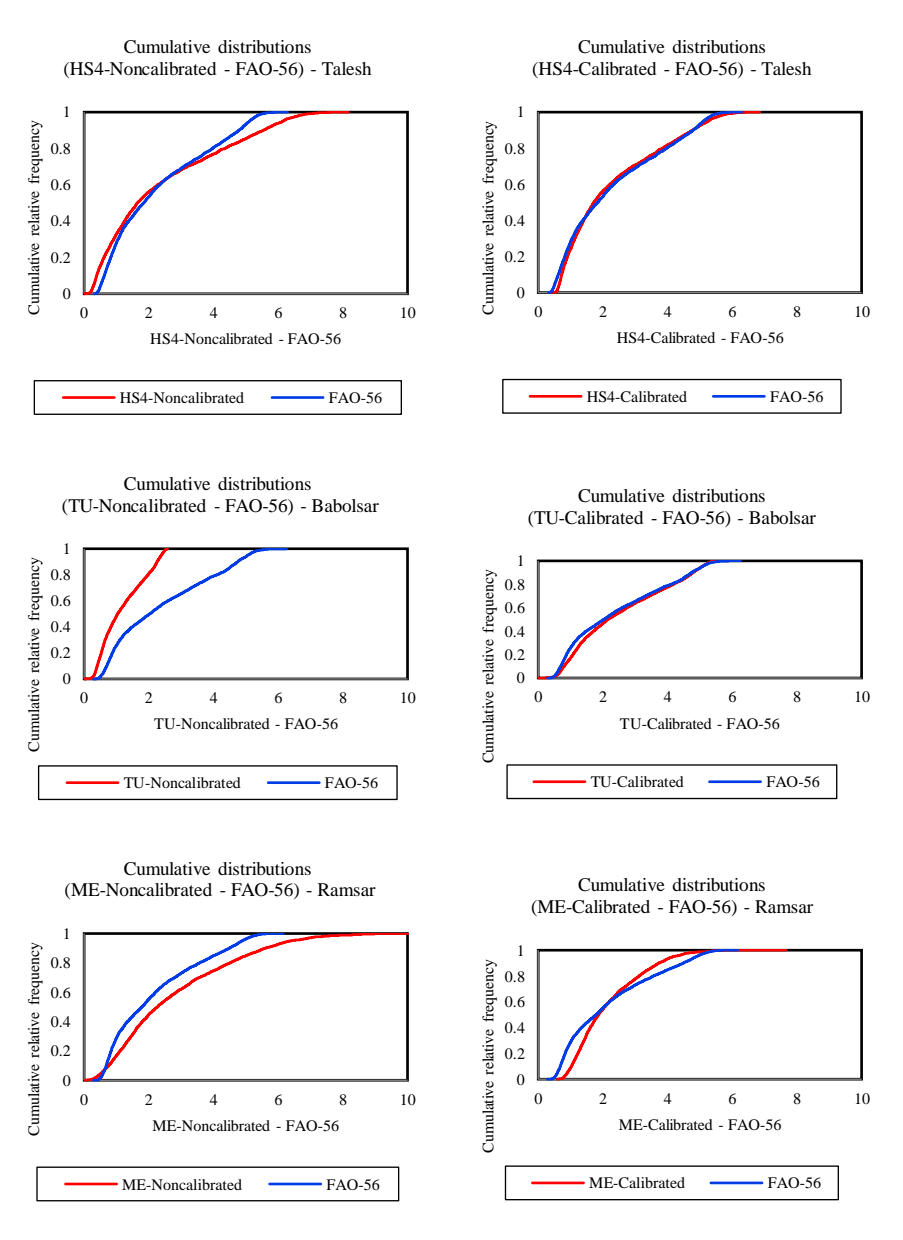


Figure 14- Cumulative distribution of the Locative calibrated models.

Conclusion

The evaluation and comparison of 15 reference evapotranspiration (ET_o) estimation models across northern Iran provided valuable insights into their accuracy, adaptability, and practical utility. Using the FAO-56 method as the benchmark, the study revealed distinct strengths and limitations across temperature-based, radiation-based, and mass transfer-based models.

- Temperature-based models: HS4 demonstrated the highest accuracy and adaptability, making it the most reliable choice for regions with limited data availability. SCH underperformed due to its reliance on wind speed, highlighting its limited applicability.
- Radiation-based models: The Turc model consistently outperformed others, offering robust performance across diverse stations. The Irmak model served as a viable secondary option, particularly in areas with high solar radiation.
- 3. Mass transfer-based models: Meyer emerged as the most accurate model in humid and coastal regions, while WMO exhibited poor performance due to its high variability and bias.

Calibration significantly enhanced the performance of all models, particularly radiation- and mass transfer-based approaches, underscoring its importance in regional adaptation. The study recommends the HS4, Turc, and Meyer models as effective alternatives to the FAO-56 method, particularly in data-scarce scenarios.

These findings provide a robust framework for selecting and applying ET_o estimation models, contributing to improved water resource management and agricultural planning in regions with diverse climatic conditions.

References

- [1] Allen, R.G., Pereira, L.S., Raes, D. & Smith, M. 1998. Crop Evapotranspiration. Guidelines for Computing Crop Evapotranspiration. FAO Irrigation and Drainage Paper, No. 56. Food and Agriculture Organization, Rome.
- [2] Antonopoulos, V.Z., Antonopoulos, A.V. 2017. Daily reference evapotranspiration estimates by artificial neural networks technique and empirical equations using limited input climate variables. Computers and Electronics in Agriculture 132, 86-96.
- [3] Bourletsikas, A., Argyrokastritis, I., Proutsos, N. 2017. Comparative evaluation of 24 reference evapotranspiration equations applied on an evergreen-broadleaved forest. Hydrology Research 49(4), 1028-1041.
- [4] Chatzithomas, C.D., Alexandris, A. 2015. Solar radiation and relative humidity based, empirical method, to estimate hourly reference evapotranspiration. Agricultural Water management 152, 188-197.
- [5] Dalton, J. 1802. Experimental essays on the constitution of mixed gases; on the force of steam of vapour from waters and other liquids in different temperatures, both in a torricellian vacuum and in air on evaporation and on the expansion of gases by heat. Mem. Manch. Lit. Philos. Soc. 5, 535–602.
- [6] Dong, J., Xing, L., Cui, N., Guo, L., Liang, C., Zhao, L., Wang, Z. and Gong, D. 2024. Estimating reference crop evapotranspiration using optimized empirical methods with a novel improved Grey Wolf Algorithm in four climatic regions of China. Agricultural Water Management. 291, 108620.
- [7] Farzanpour, H., Shiri, J., Sadraddini, A.A., Trajkovic, S. 2019. Global comparison of 20 reference evapotranspiration equations in a semi-arid region of Iran. Hydrology Research 50(1), 282-300.
- [8] Hargreaves, G.H., & Samani, Z.A. 1985. Reference crop evapotranspiration from temperature. Applied Engineering Agriculture 1, 96–99.
- [9] Irmak, S., Irmak, A., Allen, R. G., & Jones, J. W. 2003. Solar and net radiation-based equations to estimate reference evapotranspiration in humid climates. Journal of Irrigation and Drainage Engineering 129, 336– 347.
- [10] Jensen, M.E. & Haise, H.R. 1963. Estimation of evapotranspiration from solar radiation. Journal of Irrigation and Drainage Engineering 89, 15–41.
- [11] Jones, J.W. & Ritchie, J.T. 1990. Crop growth models. Management of farm irrigation systems. In: ASAE Monograph No. 9 (G. J. Hoffman, T. A. Howel & K. H. Solomon, eds). ASAE, St Joseph, MI, pp. 63–89.

- [12] Kisi, O. 2013. Comparison of different empirical methods for estimating daily reference evapotranspiration in mediterranean climate. Journal of Irrigation and Drainage Engineering 140(1),
- [13] Makkink, G.F. 1957. Testing the Penman formula by means of lysimeters. Journal of Institute of Water Engineering 11, 277–288.
- [14] Marti, P., Lopez-Urrea, R., Mancha, L., Gonzalez-Altozano, P., Roman, A. 2024. Seasonal assessment of the grass reference evapotranspiration estimation from limited inputs using different calibrating time windows and lysimeter benchmarks. Agricultural Water Management. 300, 108903.
- [15] Meyer, A. 1926. Über einige Zusammenhänge zwischen Klima und Boden in Europa. Chemie der Erde 2, 209–347.
- [16] Penman, H.C. 1948. Natural evaporation from open water, bare soil and grass. Proc. Roy. Soc. Lond. Ser. A 193, 120–145.
- [17] Priestley, C. H.B. & Taylor, R. J. 1972. On the assessment of surface heat flux and evaporation using large-scale parameters. Monthly Weather Reviews 100, 81–92.
- [18] Rohwer, C. 1931. Evaporation from free water surface. USDA Tec. Null. 217, 1–96.
- [19] Sadeghzadeh, M., shiri, J., Karimi, S. et al. 2024. Analysis of factors affecting evapotranspiration zoning. Environ Sci Pollut Res 31, 42295–42313. https://doi.org/10.1007/s11356-024-33822-9.
- [20] Schendel, U. 1967 Vegetationswasserverbrauch und-Wasserbedarf. Habilitation, Kiel, p. 137.
- [21] Sharafi, S., Mohammadi Ghaleni, M. 2021. Calibration of empirical equations for estimating reference evapotranspiration in different climates of Iran. Theoretical and Applied Climatology 145, 925-939.
- [22] Shiri, J., Nazemi, A.H., Sadraddini, A.A., Landeras, G., Kisi, O., Fakheri Fard, A. & Marti, P. 2014. Comparison of heuristic and empirical approaches for estimating reference evapotranspiration from limited inputs in Iran. Computers and Electronics in Agriculture 108, 230–241.
- [23] Tabari, H. 2010. Evaluation of reference crop evapotranspiration equations in various climates. Water Resources Management 24, 2311–2337.
- [24] Tao, H., Diop, L., Bodian, A., Djaman, K., Ndiaye, P.M., and Mundher Yaseen, Z. 2018. Reference evapotranspiration prediction using hybridized fuzzy model with firefly algorithm: Regional case study in Burkina Faso. Agricultural Water Management 208: 140-151.
- [25] Trabert, W. 1896. Neue Beobachtungen über Verdampfungsgeschwindigkeiten. Meteorology Z. 13, 261–263
- [26] Turc, L. 1961. Evaluation des besoins en eau d'irrigation evapotranspiration potentielle. Annals of Agronomy 12, 13–49.
- [27] Valle Junior et al. 2020. Comparative assessment of modelled and empirical reference evapotranspiration methods for a brazilian savanna. Agricultural Water management 232, 106040.
- [28] WMO., 1966 Measurement and Estimation of Evaporation and Evapotranspiration. Tech. Pap. (CIMO-Rep) 83. Genf. World Meteorological Organization, Geneva, Switzerland.
- [29] Zhou, H., Ma, L., Niu, X., Xiang, Y., Chen, J., Su, Y., Li, J., Lu, S., Chen, C. and Wu, Q. 2024. A novel hybrid model combined with ensemble embedded feature selection method for estimating reference evapotranspiration in the North China Plain. Agricultural Water Management. 296, 108807.